Radiative effects of reduced aerosol emissions during the COVID-19 pandemic and the future recovery

Stephanie Fiedler[1,2], Klaus Wyser[3], Joeri Rogelj[4,5], and Twan van Noije[6]

[1]University of Cologne, Institute of Geophysics and Meteorology, Cologne, Germany
[2]Hans-Ertel-Centre for Weather Research, Climate Monitoring and Diagnostics, Bonn/Cologne, Germany
[3]Rossby Centre, Swedish Meteorological and Hydrological Institute, Sweden
[4]Grantham Institute, Imperial College London, United Kingdom
[5]International Institute for Applied Systems Analysis, Laxenburg, Austria
[6]Royal Netherlands Meteorological Institute, De Bilt, Netherlands

Key Points:

- New COVID-19 data to parameterize anthropogenic aerosol properties are released for use in climate studies.
- First estimate of anthropogenic aerosol radiative forcing for 2020 suggests a change by +0.04 Wm^{-2} due to the pandemic.
- Recovery scenarios for 2050 have a spread in anthropogenic aerosol forcing of -0.38 to -0.68 Wm^{-2}.

Corresponding author: Stephanie Fiedler, stephanie.fiedler@uni-koeln.de

Abstract

The pandemic in 2020 caused an abrupt change in the emission of anthropogenic aerosols and their precursors. We provide the first estimate of the associated change in the aerosol radiative forcing at the top of the atmosphere and the surface. To this end, we perform new simulations with the contemporary Earth system model EC-Earth3 participating in CMIP6, and created new data on the anthropogenic aerosol optical properties and an associated effect on clouds for the implemented aerosol parameterization, MACv2-SP. Our results highlight the small impact of the pandemic on the global aerosol radiative forcing in 2020 compared to the baseline of the order of +0.04 $\mathrm{W m^{-2}}$, which is small compared to the natural year-to-year variability in the radiation budget. Natural variability also limits the ability to detect a meaningful regional difference in the anthropogenic aerosol radiative effects. We identify the best chances to find a significant change in radiation at the surface during cloud-free conditions for regions that were strongly polluted in the past years. The new post-pandemic recovery scenarios indicate a spread in the aerosol forcing of -0.68 to -0.38 $\mathrm{W m^{-2}}$ for 2050, which translates to a difference of +0.05 to -0.25 $\mathrm{W m^{-2}}$ compared to the baseline. This spread falls within the present-day uncertainty in aerosol radiative forcing and the CMIP6 spread in aerosol forcing at the end of the 21st century. We release the new MACv2-SP data for studies on the climate response to the pandemic and the recovery scenarios.

Plain Language Summary

Anthropogenic aerosols, released into the atmosphere due to human activities, affect the climate by scattering and absorbing sunlight and changing the properties of clouds. The socio-economic impact of the pandemic in 2020 reduced the amount on anthropogenic aerosols. We here estimate the total reduction of anthropogenic aerosols for 2020 and the implication for the radiation budget of our planet. Overall we find only a small impact on the radiation budget due to the change in anthropogenic aerosols in 2020. The post-pandemic recovery pathway influences, however, the magnitude of the total anthropogenic radiative forcing which for instance also accounts for changes in atmospheric greenhouse gas concentrations.

1 Introduction

The aerosol burden in 2020 is affected by reduced emissions of anthropogenic aerosols and their precursors associated with the global COVID-19 pandemic. Many countries have witnessed a reduction in socio-economic activities and lockdowns. The associated decline in traffic and industrial productivity have led to marked regional reductions in atmospheric pollution improving the air quality (e.g., van Heerwaarden et al., submitted; Ranjan et al., 2020). Figure 1 illustrates the change in the aerosol burden as the observed anomaly in the mid-visible aerosol optical depth, τ', for northern hemisphere spring in 2020 against the 20-year spring climatology from NASA's MODIS satellite product (Acker & Leptoukh, 2007; Platnick et al., 2015). Pronounced negative τ' in spring 2020 are identified for Eastern and Southern Asia as well as the Northwest Pacific. Even regions with typically relatively low aerosol burden like Europe and North America had less aerosol burden. The pandemic restrictions in most of the European countries for instance occurs in parallel with exceptionally blue skies and new extremes in surface irradiance (van Heerwaarden et al., submitted).

The emission reductions due to the COVID-19 pandemic are thought to potentially influence climate (e.g., Forster et al., 2020a), but the emission reductions are not considered in the contemporary climate simulations of the Coupled Model Intercomparison Project phase 6 (CMIP6, Eyring et al., 2016), used for assessing climate changes by the Intergovernmental Panel on Climate Change (IPCC). The construction of the CMIP6 scenarios of anthropogenic emissions has therefore been revisited (Forster et al., 2020b).

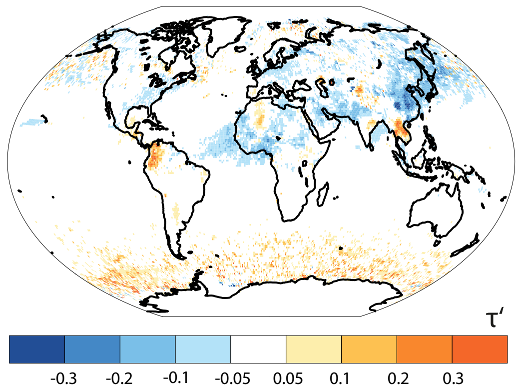

Figure 1. Observed anomaly in aerosol optical depth for northern hemisphere spring 2020. Shown is the anomaly in the aerosol optical depth (τ') at 550 nm for March–May 2020 against the climatology of the same months for 2000–2020 from MODIS.

Based on the new emission data, the scientific community plans to investigate the co-occurrence of climate anomalies and the COVID-19 impacts on global air quality. To this end, a new climate model inter-comparision project for 2015–2050 with the revised emission scenarios is planned (COVID-MIP Lamboll, et al., in prep.) under the umbrella of the Detection and Attribution Model Intercomparison Project (DAMIP, Gillett et al., n.d.) endorsed by CMIP6. Some of the participating models use the simple plumes aerosol parameterization MACv2-SP (Fiedler et al., 2017; Stevens et al., 2017) and therefore need new MACv2-SP input data consistent with the new emission data to participate in COVID-MIP. We here derive these new input data for MACv2-SP and provide it for use in climate studies.

The aim of the present study is to give a first estimate of the impact of the COVID-19 pandemic on the radiative forcing of anthropogenic aerosols for the pandemic year 2020 and the recovery scenarios from 2020 to 2050. We further derive and describe the new MACv2-SP data for the anthropogenic aerosol optical properties and an associated effect on clouds for 2015–2050 from the revised aerosol emissions (Forster et al., 2020b). These emission data cover different recovery pathways after the pandemic ranging from fossil-fuel based to green developments into the future. We use the here newly constructed MACv2-SP data in the CMIP6 model EC-Earth3 (Doescher, et al., in prep.), which uses MACv2-SP as standard to represent anthropogenic aerosols. EC-Earth3 simulates aerosol-radiation and aerosol-cloud interactions including cloud adjustments from MACv2-SP. We perform new atmosphere-only experiments with EC-Earth3 and estimate the effective radiative forcing (ERF) of the anthropogenic aerosols in 2020 and 2050 for both the top of the atmosphere and the surface. Details of our methods are given in Section 2, followed by our results in Section 3, and our conclusions in Section 4.

2 Methods

2.1 Emissions of SO_2 and NH_3

Forster et al. (2020b) developed five scenarios to explore the impact of the COVID-19 pandemic on current and future emissions. These scenarios are:

- A baseline scenario (*base*) without any impact of the COVID-19 pandemic and the measures to contain it;

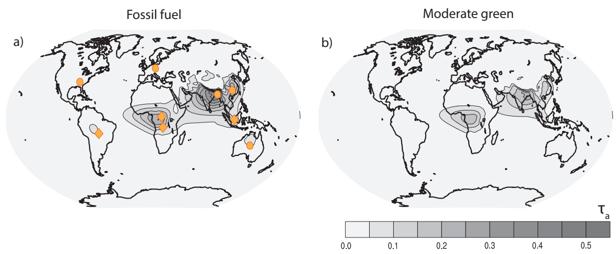

Figure 2. MACv2-SP τ_a in 2050. Shown is the annual mean in anthropogenic aerosol optical depth (τ_a) at 550 nm for the (a) fossil-fuel based, (b) moderate green, and (c) strong green scenario. Orange symbols mark the centers of the aerosol plumes associated with industrial pollution (circles) and emissions from both industry and biomass burning (rectangles).

- A two-year-blip scenario (*blp*) that assumes emissions return to the baseline scenario after a two-year reduction in emissions due to temporary societal lockdowns and disruptions;
- A fossil-fuel recovery scenario (*ff*) that assumes the recovery from the COVID-19 economic downturn preferentially supports polluting fossil-fuel-based economic sectors;
- A moderate and strong green recovery scenario (called *mg* and *sg*, respectively) that assume different levels of preferential stimulus of green sectors during the recovery from COVID-19 (e.g., see Andrijevic et al. (2020)) that would lead to limiting global mean temperature increase relative to preindustrial levels to well below $2°C$ and to $1.5°C$, respectively (Forster et al., 2020b).

The near-term evolution of SO_2 and NH_3 during the COVID-19 lockdown period uses the activity scaling method of (Forster et al., 2020b). For the extensions beyond the COVID-19 lockdown period and until 2050, the large-scale global relationships between greenhouse gases, aerosols and aerosol precursors as found in detailed emissions scenarios derived with integrated assessment models were used (Lamboll et al., 2020). Emissions evolutions of SO_2 and NH_3 compatible with each of the above scenario have been estimated, based on the relationships found in the scenario ensemble compiled and assessed as part of the Intergovernmental Panel on Climate Change's (IPCC) Special Report on Global Warming of $1.5°C$ (Rogelj et al., 2018; Huppmann et al., 2018).

2.2 Anthropogenic aerosol parameterization

We use the emissions of SO_2 and NH_3 from Forster et al. (2020b) to create the new input data for the novel simple-plumes parameterization MACv2-SP (Fiedler et al., 2017; Stevens et al., 2017) in use for representing anthropogenic aerosol effects in climate models of CMIP6 ¡e.g.,¿Mauritsen2019. MACv2-SP prescribes month-to-month and year-to-year changes of the three dimensional fields of anthropogenic aerosol optical properties and associated effects on clouds. Temporal changes from 1850 to 2100 have been derived by scaling the anthropogenic aerosol optical depth of 2005 with the CMIP6 emission amounts of SO_2 and NH_3 (Stevens et al., 2017; Fiedler et al., 2019b). This scaling did not account for the effect of the pandemic on anthropogenic emissions. We therefore create here new MACv2-SP input data, based on the new emission data sets for 2015–2050, which account for the COVID-19 pandemic and four recovery scenarios (Forster et al., 2020b).

For creating the new MACv2-SP data, we scale the anthropogenic aerosol optical depth and the effect on clouds from 2005 to other years by multiplying scaling factors

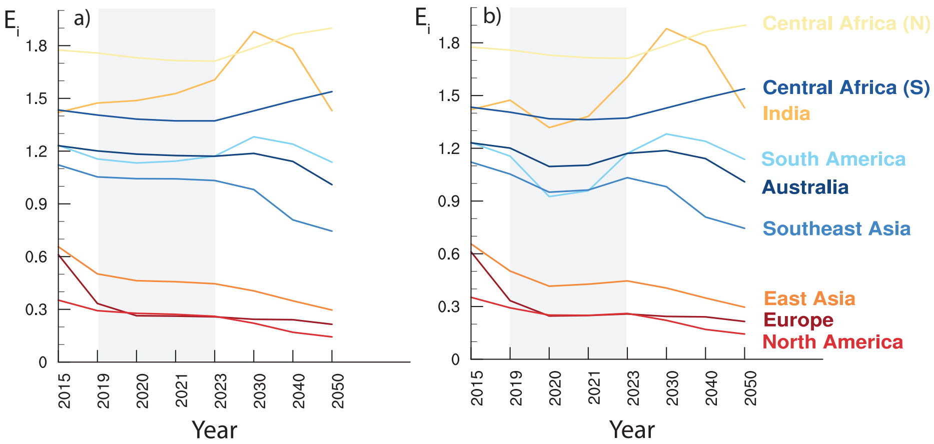

Figure 3. Example of the scaling factors for the aerosol optical depth in the centre of the aerosol plumes for two scenarios. Shown are the annual scaling factors for the color-coded plumes calculated from the (a) baseline and (b) two-year-blip emission data for the years provided in the data. The pandemic period 2019–2023 is marked with grey shading.

in the centre of the plumes, marked in Figure 2a. Mathematical functions in MACv2-SP use the values in the plume centers to create the three dimensional distribution of the aerosol extinction. As an example, Figure 2 shows the maps of the mid-visible anthropogenic aerosol optical depth in 2050 from MACv2-SP for three scenarios that we derive here. Technically, we create annual scaling factors for each plume center and each year to be represented in MACv2-SP. A comprehensive technical description of MACv2-SP is given by Stevens et al. (2017).

Our method for constructing the scaling factors for MACv2-SP is similar to the method for the CMIP6 scenarios (Fiedler et al., 2019b). The anthropogenic aerosol optical depth τ_i in each plume center $i = 1, ..., 9$ is scaled with the emission scaling factor E_i for the years t with:

$$\tau_i(t) = E_i(t)\tau_i(2005) \tag{1}$$

We use $\tau_i(2005)$ at 550 nm from Stevens et al. (2017). The scaling factors $E_i(t)$ are constructed from the anthropogenic emission ϵ_{ik} of the species k. These are the gridded emission data for SO_2 and NH_3 from the emission data version 4 (Forster et al., 2020b). The calculation of $E_i(t)$ follows Fiedler et al. (2019a):

$$E_i(t) = \frac{\sum_{k-1,2} w_k[\epsilon_{ik}(t) - \epsilon_{ik}(1850)]}{\sum_{k-1,2} w_k[\epsilon_{ik}(2005) - \epsilon_{ik}(1850)]} \tag{2}$$

The emissions of 1850 and 2005 are taken from the CMIP6 historical emission data. We consider emissions from all anthropogenic sectors provided by Forster et al. (2020b), and include open burning emissions from the CMIP6 scenario SSP2-45. SSP2-45 is the baseline for the experiments to be carried out in COVID-MIP (Lamboll, et al., in prep.). The anthropogenic emissions ϵ_{ik} are integrated values over the 10x10 grid boxes surrounding the plume center. The weights w_k for the two species are $w_1 = 0.645$ for SO_2 and $w_2 = 0.355$ for NH_3, representing the forcing ratio of sulphate against ammonia for present day (Stevens et al., 2017).

Figure 3 shows examples of the scaling factors for each of the nine aerosol plume centers i. Contrasting the baseline against the two-year-blip data illustrates the reduction of E_i for 2020–2021. The reduction for E_i is particularly strong for the plumes over

India and South America. Comparably smaller changes are seen in areas where the anthropogenic aerosol burden has been relatively small in the past decade, i.e., Europe and North America, and where biomass burning contributes more to the aerosol burden than other anthropogenic sources, namely in the African plumes.

MACv2-SP typically uses one $E_i(t)$ per decade with linear interpolation in between. This is the same here, except that we also construct the scaling factors for the individual years around 2020 for consistency with the COVID-19 emission data. We note that the observed small-scale structures in the aerosol burden, e.g., like in local observations, cannot be created with MACv2-SP owing to the design and purpose of this parameterization (Stevens et al., 2017). As such results from using these individual years in later studies should be interpreted as estimates for the large-scale influence and not as local constraints of the forcing for individual years.

Aerosol absorption is prescribed with the single scattering albedo of $\omega_0 = 0.93$ for industrial plumes and $\omega_0 = 0.87$ for plumes additionally affected by biomass burning, marked in Figure 2a. The asymmetry parameter, $\gamma = 0.63$, is constant. MACv2-SP uses the Angstrom exponent $\alpha = 2$ to interpolate the aerosol optical properties for different wavelengths.

Additionally to the aerosol optical properties, MACv2-SP prescribes aerosol effects on the cloud droplet number concentrations N. The latter is induced with the prefactor η_N to be multiplied with N in the host model:

$$\eta_N = 1 + \frac{dN}{N} = \frac{ln[1000(\tau_a(\phi,\lambda,t) + \tau_b(\phi,\lambda,t)) + 1]}{ln[1000\tau_b(\phi,\lambda,t) + 1]} \tag{3}$$

The background aerosol optical depth (τ_b) is a simplified representation that follows the plume structure for τ_a to parameterize the aerosol effect on clouds. Host models can multiply η_N with N in the radiation transfer calculation to induce a Twomey effect only, e.g., in MPI-ESM1.2, or in the cloud microphysics to allow further rapid adjustments of clouds, e.g., in EC-Earth3. Additional documentation of MACv2-SP and details on the application in climate studies is given elsewhere (e.g., Fiedler et al., 2017; Stevens et al., 2017; Fiedler et al., 2019a).

The new MACv2-SP input data are provided as supplementary material for use in climate studies, e.g., in COVID-MIP (Lamboll, et al., in prep.). It covers the baseline and scenarios that assume recoveries after COVID-19 that intensify the use of fossil fuels, follow a moderate or strong green pathway, and return to a business as usual pathway after the assumed two-year interruption by the pandemic in 2020 and 2021.

2.3 Model experiment strategy

We estimate the ERF of the anthropogenic aerosol reduction in 2020 and the ERF spread associated with the recovery scenarios in 2050 from the new data. To this end, we perform atmosphere-only simulations with EC-Earth3 and compute the ERF of the anthropogenic aerosols at the top of the atmosphere and the surface, i.e., the instantaneous radiative effects plus the rapid adjustments in the atmosphere. EC-Earth3 is an Earth system model participating in CMIP6. It is based on the atmosphere and land-surface model from ECMWF's IFS cycle 36r4, and the ocean and sea-ice model NEMO version 3.6. The implementation of MACv2-SP in EC-Earth3 (Doescher, et al., in prep.) is such that the model accounts for aerosol-radiation interactions and aerosol-cloud interactions, including aerosol albedo and cloud lifetime effects (Fiedler et al., 2019a).

Our simulations use annually repeating aerosol optical properties and associated effects on clouds for the years 2020 and 2050. We run experiment with the setups:

Table 1. Global means from the new MACv2-SP data and EC-Earth3 experiments. Shown are the ERF at the top of the atmosphere (ERF_{TOA}) and at the surface (ERF_{SFC}) calculated against *pi* as the mean ± 95% confidence interval. (*) marks differences to the baseline that are statistically significant at the 95 % level.

Experiment	$\overline{\tau_a}$	$\overline{\eta_N}$	ERF_{TOA} [$\mathrm{Wm^{-2}}$]	ERF_{SFC} [$\mathrm{Wm^{-2}}$]
2020-base	0.021	1.060	-0.661 ± 0.087	-1.449 ± 0.047
2020-blp	0.019	1.056	-0.622 ± 0.072	-1.338 ± 0.038 (*)
2050-base	0.019	1.054	-0.631 ± 0.068	-1.324 ± 0.035
2050-ff	0.020	1.057	-0.675 ± 0.081	-1.409 ± 0.041 (*)
2050-mg	0.012	1.038	-0.382 ± 0.080 (*)	-0.875 ± 0.036 (*)
2050-sg	0.014	1.040	-0.461 ± 0.069 (*)	-0.987 ± 0.039 (*)

- *base*: new MACv2-SP properties from the baseline for the year 2020 (*2020-base*) and 2050 (*2050-base*) .
- *2020-blp*: new MACv2-SP properties from the two-year-blip for 2020,
- *2050*: new MACv2-SP properties for 2050 from the recovery scenarios that are either primarily fossil-fuel based (*2050-ff*), moderate (*2050-mg*) or strong green (*2050-sg*), and
- *pi*: without anthropogenic aerosol effects for calculating the ERF in 2020 and 2050 relative to the pre-industrial.

The setup of the experiments follows Wyser et al. (2020) and is identical except for the listed changes in the anthropogenic aerosols. We use a pre-industrial experiment setup, as typical for radiative forcing calculations from contemporary climate model experiments (Pincus et al., 2016; Fiedler et al., 2019a; Smith et al., 2020). This means we prescribe annually repeating pre-industrial boundary conditions in atmosphere-only experiments like for a *piClim-control* experiment in the Radiative Forcing Model Inter-comparison project (RFMIP, Pincus et al., 2016), i.e., a monthly climatology for sea-surface temperatures and sea ice derived from the model's pre-industrial control experiments for CMIP6. All simulations are run for 55 years. The first 5 simulation years are discarded in our analyses. We compute 50-year averages for ERF to eliminate the impact of natural year-to-year variability on the estimate (Fiedler et al., 2019a).

3 Results

3.1 Annual means of τ_a and η_N

We show the global annual means of the anthropogenic aerosol optical depth ($\overline{\tau_a}$) and the prefactor for inducing aerosol effects on clouds ($\overline{\eta_N}$) in Figure 4. Both $\overline{\tau_a}$ and $\overline{\eta_N}$ clearly reduce during the pandemic, e.g., by 0.002 for 2020 compared to the baseline and by 0.005 compared to 2005. These translate to a reduction by about 10% and 25% for the global $\overline{\tau_a}$ in 2020 and 2050. The associated effect on $\overline{\eta_N}$ is consistent with the change in $\overline{\tau_a}$, with a reduction of $\overline{\eta_N}$ by 0.004 compared to baseline and 0.017 compared to 2005, i.e., a global reduction in η_N by about 0.5–1%. All data sets have the same emissions for 2015–2023, except the baseline. Hence results from MACv2-SP other than the baseline are identical with the two-year-blip results for this period (Figure 4 and Table 1).

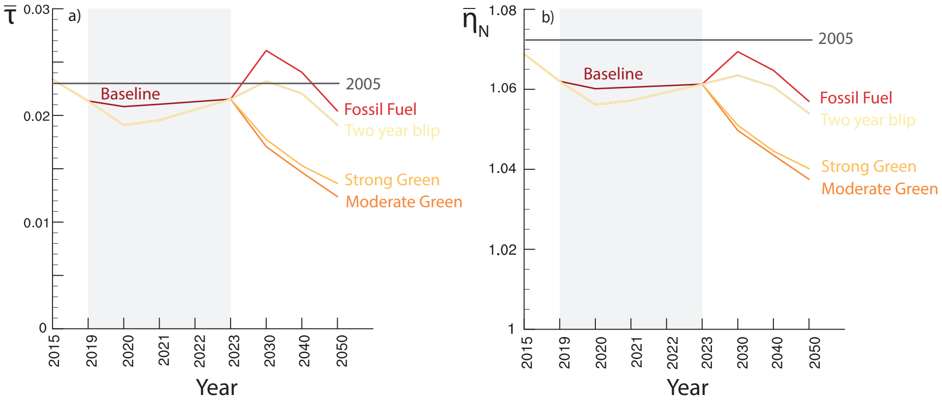

Figure 4. MACv2-SP τ_a in 2015–2050. Shown are the global annual means in (a) the anthropogenic aerosol optical depth (τ_a) at 550 nm and (b) the scaling factor the cloud droplet number concentration (η_N) for the scenarios. The pandemic period 2019–2023 is marked with grey shading. The baseline and two-year blip scenario overlap for 2030–2050. All scenarios except baseline overlap for 2015–2030. The 2005 value from the historical scaling is marked as horizontal line.

The post-pandemic recovery of τ_a and η_N strongly depends on the scenario. The $\overline{\tau_a}$ in 2030 is close to the value in 2005 in the baseline and two-year-blip scenario, larger in the fossil fuel scenario, and substantially smaller for both green scenarios (Figure 4). By 2050 all scenarios point to a decrease of $\overline{\tau_a}$ relative to 2005, with the strongest reduction in the moderate green not the strong green scenario. This might be counter intuitive since a stronger green scenario might suggest cleaner air. The smaller $\overline{\tau_a}$ in the moderate green scenario is due to the lower emissions of NH_3 compared to the strong green by about -3.5$\times10^{-6}$ kg m^{-2} s^{-1} in 2050, integrated over the globe and sectors. Although the emissions of SO_2 are smaller in the strong green scenario, the total effect of NH_3 and SO_2 on the scaling factor E_i (Section 2) leads to a slightly larger $\overline{\tau_a}$ in the strong green scenarios.

The assumption of larger NH_3 emissions in the strong green recovery scenario compared to the moderate green recovery scenario is the result of changes in the structure of the economy in low emissions scenarios, particularly related to agricultural practice and energy provision. Stringent emissions scenarios to an increasing degree rely on more efficient food and biomass production to support a growing world population while generating low-carbon energy and enable possibilities of carbon-dioxide sequestration (Popp et al., 2017). The fertilizer use required to achieve this results in an increase in NH_3 emissions. Furthermore, stringent climate change mitigation scenarios often rely on very high shares of renewable energy, which have intermittent power generation properties and thus require energy storage technologies to bridge gaps in supply. One energy storage technology that can store energy across seasons and even multiple years is associated with NH_3 emissions (Society, 2020). The projected increased use of ammonia, as a fuel and for energy storage, results in larger projected emissions of NH_3 due to leakage and due to imperfect transport or storage. Slightly higher NH_3 emissions in the strong green (sg) than the moderate (mg) recovery scenarios are hence consistent with the general understanding of the technologies and practices that would be required for a transformation to a strongly decarbonized society.

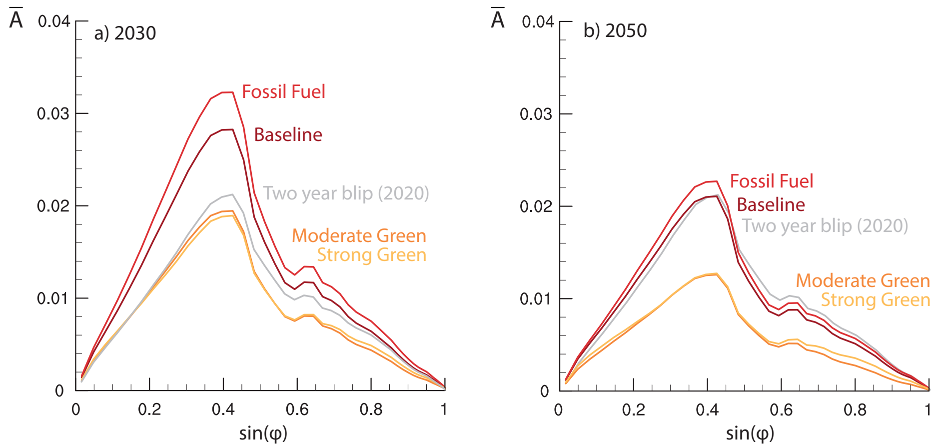

Figure 5. Hemispheric asymmetry for τ_a. Shown is the hemispheric asymmetry (A) as function of the sinus of the geographical latitude for (a) 2030 and (b) 2050 for all scenarios. Baseline and two-year blip are identical for these years. We mark the values of the two-year blip scenario in 2020 as a reference.

3.2 Hemispheric asymmetry in τ_a

The spatial distribution of τ_a, measured by the hemispheric asymmetry, is qualitatively similar across the scenarios, but the magnitudes differ. Figure 5 illustrates the hemispheric asymmetry A:

$$A = \frac{\overline{\tau_a(\phi)} - \overline{\tau_a(-\phi)}}{2} \tag{4}$$

using the zonal averages $\tau_a(\phi)$ at the same geographical latitudes on the northern (ϕ) and southern hemisphere ($-\phi$). All scenarios have larger A in the tropics and sub-tropics than further poleward (Fig. 5), consistent with the CMIP6 scenarios (Fiedler et al., 2019a). For 2030, the fossil fuel and baseline scenarios have substantially higher A than for 2020. In the middle of the 21st century, A in the fossil fuel and baseline scenarios are more similar to each other and close to A from 2020.

The temporal behaviour for A in the green scenarios is opposite to the fossil-fuel dominated scenarios, i.e., they are close to A from 2020 in 2030 and differ in 2050. Both green scenarios in 2030 have particularly similar A to 2020 in the tropics and slightly larger differences poleward. In 2050, the green scenarios are still similar to each other, but have overall smaller A compared to 2020, e.g., a reduction by 50% in the maximum around $\phi = 24°$. This reflects the decrease in τ_a due to improved air quality in a green recovery (compare Fig. 4).

3.3 Seasonal cycle in τ_a

The month-to-month changes in τ_a from MACv2-SP is dominated by the biomass burning seasons. These lead to tropical maxima in τ_a between July and October and November and February (Fig. 6a–b). From the sub-tropics to the poles, the seasonal cycle in the scenarios slightly differ from the baseline for 2020. Note here again that all data sets are identical with the two-year-blip in 2020, except the baseline. Overall, the seasonal and zonal patterns are very similar, e.g., seen with the weighting by the global τ_a (Fig. 6c–d) with only marginal changes as we go towards 2050 (not shown).

In 2050, the overall seasonal pattern in τ_a remains qualitatively similar, but the magnitudes strongly depend on the scenario. The green scenarios show the largest re-

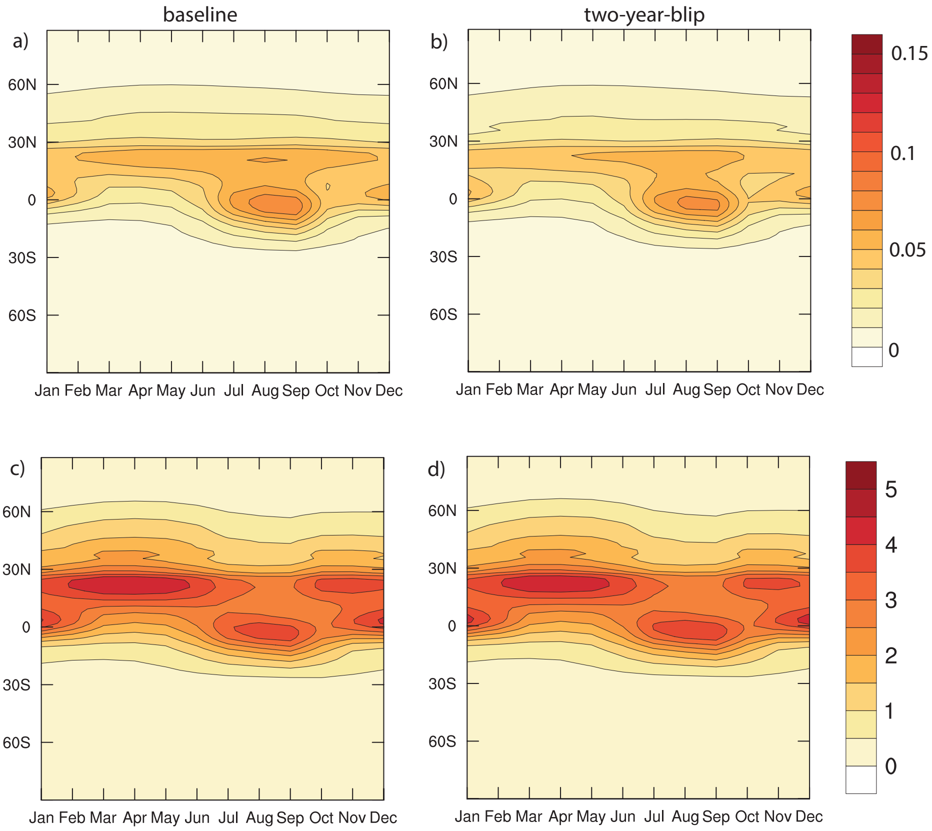

Figure 6. MACv2-SP τ_a patterns in 2020. Shown are the annual cycles of the anthropogenic aerosol optical depth (τ_a) at 550 nm as (top) zonal means and (bottom) zonal means weighted by $\overline{\tau_a}$ for the (left) baseline, and (right) two-year-blip scenario.

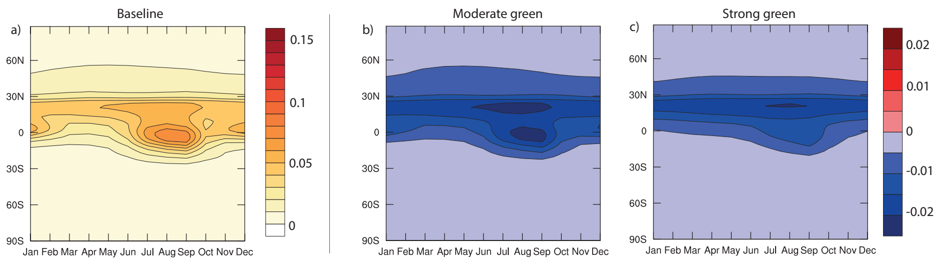

Figure 7. MACv2-SP τ_a patterns in 2050. Shown is the annual cycles of the anthropogenic aerosol optical depth (τ_a) at 550 nm as (a) zonal mean for the baseline, and (b–c) difference of the green scenarios relative to baseline for 2050.

ductions in τ_a that are primarily projected in the northern hemisphere equatorward of 50°N. Here, the strongest reductions occur between June and October in the moderate green scenario. Again the stronger reduction in τ_a in the moderate than the strong green scenario is associated with the larger emissions of NH_3 in the strong green recovery leading to larger τ_a than for the moderate green scenario.

3.4 Global radiative forcing

We calculate the global ERF of anthropogenic aerosols from our experiments with the new MACv2-SP data at the top of the atmosphere and at the surface, ERF_{TOA} and ERF_{SFC}. For 2020, the impact of the reduction in anthropogenic aerosols compared to the baseline is a less negative ERF_{TOA} by about +0.04 Wm^{-2} (Table 1). This reduction is small compared to the the year-to-year variability in the model, reflected by the confidence intervals about the mean of ±0.07 Wm^{-2} to ±0.09 Wm^{-2} across our ensemble of model simulations. Again these estimates are based on fifty years of simulations with annually repeating aerosol patterns. It will therefore be difficult to disentangle any differences in the TOA radiation budget due to reductions in aerosols during the pandemic from differences arising due to natural variability in both observations and small ensembles of simulations. We identify a larger and statistically significant difference in ERF_{SFC} associated with the aerosol reduction during the pandemic compared to the baseline of the order of 0.1 Wm^{-2} (Table 1). This implies that radiation observations at the surface and sufficiently many model estimates for ERF_{SFC} can be more informative for quantifying the influence of the pandemic on the global radiation and energy budget than estimates for the TOA.

The spread in ERF_{TOA} of anthropogenic aerosols due to the different scenarios for 2050 is -0.68 Wm^{-2} to -0.38 Wm^{-2} (Table 1). Compared to the baseline, these are differences of +0.05 to -0.25 Wm^{-2}. The least negative ERF_{TOA} occurs for the moderate green scenario, consistent with the lowest τ_a across the MACv2-SP data associated with the lower NH_3 emissions than in the strong green scenario. We obtain ERF_{TOA} of the anthropogenic aerosols for the green scenarios that are statistically significant different compared to the baseline. Baseline and the fossil-fuel based scenarios, however, yield very similar ERF_{TOA} for 2050, consistent with small differences in $\overline{\tau_a}$ and $\overline{\eta_N}$ for the two scenarios (Figure 8a). The ERF_{SFC} for 2050 is more negative than ERF_{TOA} (Figure 8b) and has a smaller 95 % confidence interval of about ± 0.04 Wm^{-2} compared to ERF_{TOA}. We therefore find for all scenarios a statistically significant difference in ERF_{SFC} relative to 2050-base (Table 1).

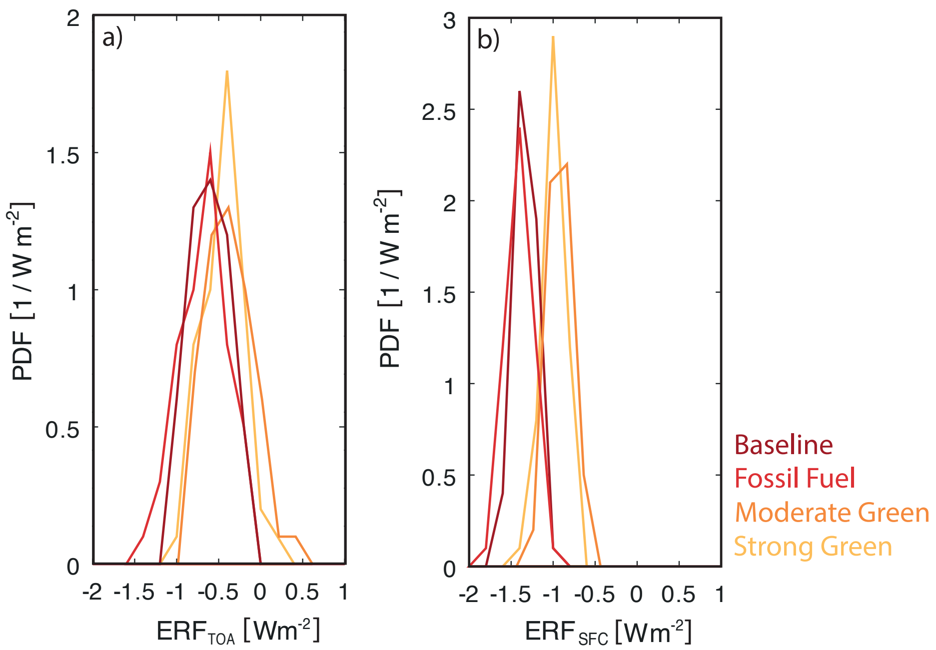

Figure 8. Probability density function for the global mean ERF in 2050. Shown are the occurrence frequency of annual mean ERF at (a) the top of the atmosphere (TOA) and (b) the surface (SFC) for the color-coded scenarios in 2050. ERF is calculated from 50 years of data from our EC-Earth3 experiments with anthropogenic aerosols (*2050-base*, *2050-ff*, *2050-mg*, *2050-sg*) against the pre-industrial control experiment (*pi*).

3.5 Pattern of radiative effects

We assess the spatial distribution of the radiative effects associated with the anthropogenic aerosols. To this end, we calculate the effective radiative effects in all-sky (F_{all}), clear-sky (F_{clr}), and cloudy-sky (F_{cld}) using the relationship:

$$F_{all} = (1 - f)F_{clr} + fF_{cld}, \tag{5}$$

with the total cloud cover (f). Figure 9 and 10 show the results for the top of the atmosphere (TOA) and at the surface.

For 2020, we find some evidence for regionally significant differences in the radiative effects at TOA associated with anthropogenic aerosol reductions due to the pandemic, but the spatial extent of these regions is typically small in F_{all} (Figure 9). This is primarily explained by the strong variability of clouds, leading to only limited areas offshore of major pollution with a significant increase in F_{cld}, hence a less negative (weaker) F_{cld} due to the pandemic. The signal for F_{clr} at TOA is more distinct, and indicates less negative radiative effects over larger regions, e.g., offshore of typically polluted regions in Asia. At the surface, the regional differences in the described radiative effects are more pronounced and spatially further extended, covering large parts in Southeast Asia and East Asia both over land and ocean. Surface measurements in these regions could potentially help to constrain the aerosol effects on climate. Much of the radiative effects occur over oceans, where the measurement network is typically sparse. Efforts to collect necessary observations during this unique situation could involve sun photometer measurements aboard research vessels as part of the Maritime Aerosol Network (e.g., Smirnov et al., 2009) and in-situ measurements aboard aircrafts based on existing expertises (e.g., Zuidema et al., 2016).

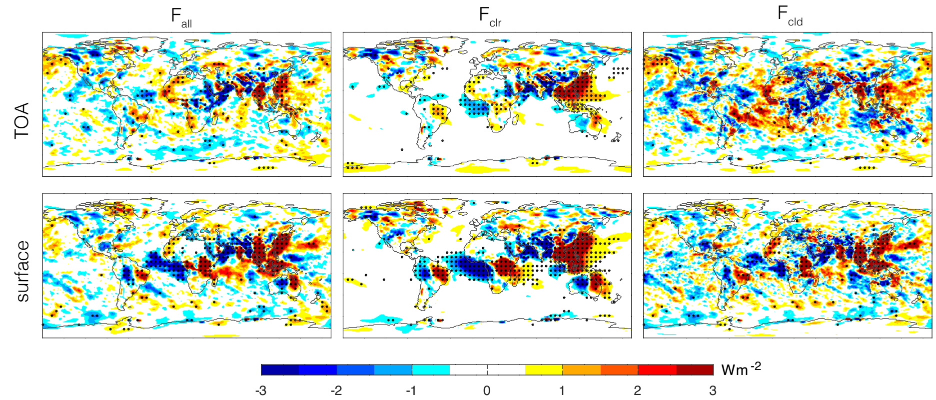

Figure 9. Differences in effective radiative effects due to the pandemic in 2020. Shown are differences between *2020-blp* and *2020-base* for the effective radiative effects in (left) all-sky (F_{all}), (middle) clear-sky (F_{clr}) and (right) cloudy-sky (F_{cld}) at (top) the top of the atmosphere and (bottom) the surface. Black dots mark regions where the differences are statistically significant at the 95 % confidence level.

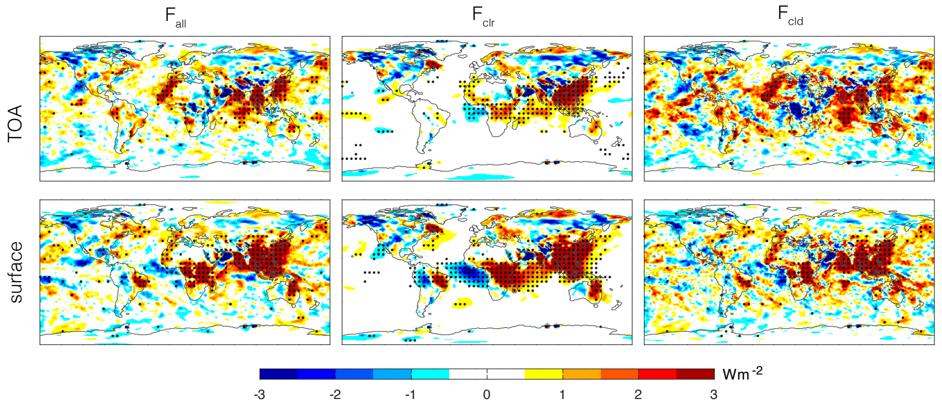

Figure 10. As Fig. 9 but for the differences between the moderate green (*2050-mg*) against the baseline (*2050-base*) scenario in 2050.

The scenario differences in F_{all} at TOA for 2050 are largest in South, Southeast and East Asia (Figure 10). Here, F_{clr} shows significant differences with less negative radiative effects in the moderate green scenario compared to the baseline by up to 3 Wm^{-2}. The pattern of F_{cld} is again more inhomogeneous than F_{clr}. The overall pattern for F_{all} differences at the surface is again qualitatively similar, but the magnitude and spatial extent are larger. Based on these results, significant scenario differences for the radiative effects associated with anthropogenic aerosols are primarily confined to the tropics and sub-tropics close to hotspots for industrial activity at present.

4 Conclusion

We show the anthropogenic aerosol optical properties and the associated effect on clouds based on the new COVID-19 emission data. Our results point to a reduction in the global anthropogenic aerosol optical depth by 10% due to the pandemic compared to the baseline. Scenarios for the post-pandemic recovery indicate a continuous increase in aerosols until 2030 in half of the scenarios and a general decrease for 2030—-2050. The spread in the anthropogenic aerosol optical depth in 2050 is 0.012 to 0.02, which is lower than in 2005. These values fall within the lower end of the spread in 2050 obtained from the original CMIP6 aerosol scenarios (Fiedler et al., 2019b).

First estimates of the effective radiative forcing (ERF) associated with the new anthropogenic aerosols are calculated from several hundred years of atmosphere-only simulations with EC-Earth3. The results highlight a weaker (less negative) aerosol ERF of the order of 10% during the pandemic relative to the baseline. Such small ERF differences require long averaging, hence our 50 years of simulations for each aerosol pattern assessed here. The small change in aerosol ERF for the time of the pandemic is not expected to induce a global climate response that is clearly detectable in light of model-internal variability. Even regional radiative effects are rather difficult to detect at the top of the atmosphere. We find, however, more significant effective radiative effects at the surface in regions typically more strongly polluted by aerosols. Any attempt to use the pandemic period to constraint aerosol effects should therefore focus on areas in South and East Asia, primarily focusing on effects at the surface. This may involve station observations, but our experiments suggest that much of the aerosol signal is expected offshore of land with major pollution in the past decades. We therefore propose to also use other measurements, e.g., from sun photometers aboard research vessels or in-situ instruments aboard aircrafts. Measurements outside of clouds might be particularly beneficial, although much research focuses on aerosol-cloud interactions. Our model results indeed suggest that there are better chances to obtain a signal in clear sky conditions at the surface rather than in cloudy and all sky. We mostly find poor prospects to measure a meaningful regional effect on clouds due to the strong influence of natural variability.

For 2050, we obtain an ERF spread of -0.68 to -0.38 Wm^{-2}, which is smaller than the ERF from the same model for 2005 and 1975 (Fiedler et al., 2019a). These ERF estimates for 2050 fall within the ERF spread for 2095 associated with the emission pathways from CMIP6 and uncertainty in aerosol-cloud interactions (Fiedler et al., 2019b). Interestingly, the stronger green scenario does not yield the smallest anthropogenic aerosol optical depth and least negative forcing, but the moderate green recovery does. This is associated with a relative increase in NH_3 emissions due to intense land-use paired with an energy system primarily relying on renewable sources. Such a pathway implies a slightly stronger warming due to weaker aerosol cooling in the strong green than the moderate green scenario. We expect, however, a stronger reduction in greenhouse gas emissions in the strong green pathway. Taken together the anthropogenic warming in the strong green scenario is therefore expected to be the weakest. Regionally, our simulations suggest the largest differences in the aerosol radiative effects across sub-tropical and tropical regions.

Our global ERF estimates for the anthropogenic aerosols fall within the plausible range of the present-day aerosol ERF (Bellouin et al., 2020) underlining the still large uncertainty in our understanding of aerosol effects compared to our ability to estimate a change in ERF from different emission pathways from a complex model. We expect that models participating in COVID-MIP will show diversity in their aerosol ERF owing to model-internal variability and model biases, even when they use the same emissions or MACv2-SP data (e.g., Fiedler et al., 2019a; Smith et al., 2020). Reasons for the model diversity in aerosol ERF include not only uncertainties in the aerosol parameterizations, but also the ability of the host model to accurately simulate important processes influencing the aerosol life cycle and therefore ERF, e.g., the parameterization of clouds and the representation of circulation. Future research should therefore also address the relative contributions from host model biases to the model diversity in ERF, e.g., using simulations performed in the framework of the Radiative Forcing Model Inter-comparison Project (RFMIP, Pincus et al., 2016) endorsed by CMIP6.

Acknowledgments

SF acknowledges the funding from the German Research Foundation for the Collaborative Research Centre 1211 (ID: DFG 268236062, `https://sfb1211.uni-koeln.de`) and from the German Federal Ministry for Transportation and Digital Infrastructure for the Hans-Ertel-Centre for Weather Research (ID: BMVI/DWD 4818DWDP5A, `https://www.herz.uni-bonn.de`). KW and TvN received support from European Union's Horizon 2020 research and innovation programme under grant agreement No 821205 (FORCeS).

Processed MODIS satellite data for the aerosol optical depth was downloaded from the Giovanni online data system (MOD08_M3 v6.1, `https://giovanni.gsfc.nasa.gov/`, accessed 4 September 2020), developed and maintained by the NASA GES DISC. We also acknowledge the MODIS mission scientists and associated NASA personnel for the production of the data shown in this article. The MACv2-SP code and input data are freely accessible in the supplement of previous (Stevens et al., 2017; Fiedler et al., 2019a) and this article. The EC-Earth3 simulations were performed on resources provided by the Swedish National Infrastructure for Computing (SNIC) at NSC. The results from the EC-Earth3 simulations used in this study are available from Wyser (2020).

References

Acker, J. G., & Leptoukh, G. (2007). *Online Analysis Enhances Use of NASA Earth Science Data.* Retrieved from `https://giovanni.gsfc.nasa.gov`

Andrijevic, M., Schleussner, C.-F., Gidden, M. J., McCollum, D. L., & Rogelj, J. (2020, Oct). Covid-19 recovery funds dwarf clean energy investment needs. *Science*, *370*(6514), 298–300. doi: 10.1126/science.abc9697

Bellouin, N., Quaas, J., Gryspeerdt, E., Kinne, S., Stier, P., Watson-Parris, D., ... Stevens, B. (2020). Bounding global aerosol radiative forcing of climate change. *Reviews of Geophysics*, *58*(1), e2019RG000660. Retrieved from `https://agupubs.onlinelibrary.wiley.com/doi/abs/10.1029/2019RG000660` doi: 10.1029/2019RG000660

Doescher. (n.d.). *et al., The community Earth system model EC-Earth for collaborative climate research, in prep.*

Eyring, V., Bony, S., Meehl, G. A., Senior, C. A., Stevens, B., Stouffer, R. J., & Taylor, K. E. (2016). Overview of the Coupled Model Intercomparison Project Phase 6 (CMIP6) experimental design and organization. *Geosci. Model Dev.*, *9*(5), 1937–1958. doi: 10.5194/gmd-9-1937-2016

Fiedler, S., Kinne, S., Huang, W. T. K., Räisänen, P., O'Donnell, D., Bellouin, N., ... Lohmann, U. (2019a). Anthropogenic aerosol forcing – insights from multi-estimates from aerosol-climate models with reduced complexity. *Atmospheric Chemistry and Physics*, *19*, 6821–6841. doi: 10.5194/acp-19-6821-2019

Fiedler, S., Stevens, B., Gidden, M., Smith, S. J., Riahi, K., & van Vuuren, D. (2019b). First forcing estimates from the future CMIP6 scenarios of anthropogenic aerosol optical properties and an associated Twomey effect. *Geoscientific Model Development*, *12*, 989–1007. doi: 10.5194/gmd-12-989-2019

Fiedler, S., Stevens, B., & Mauritsen, T. (2017). On the sensitivity of anthropogenic aerosol forcing to model-internal variability and parameterizing a Twomey effect. *J. Adv. Model. Earth Syst.*, *9*, n/a–n/a. doi: 10.1002/2017MS000932

Forster, P. M., Forster, H. I., Evans, M. J., Gidden, M. J., Jones, C. D., Keller, C. A., ... Turnock, S. T. (2020a). Current and future global climate impacts resulting from covid-19. *Nature Climate Change*. Retrieved from `https://doi.org/10.1038/s41558-020-0883-0` doi: 10.1038/s41558-020-0883-0

Forster, P. M., Lamboll, R., & Rogelj, J. (2020b). *Emissions changes in 2020 due to covid19.* Zenodo. doi: 10.5281/zenodo.3957826

Gillett, N. P., Shiogama, H., Funke, B., Hegerl, G., Knutti, R., Matthes, K., ... Tebaldi, C. (n.d.). the detection and attribution model intercomparison project (damip v1.0) contribution to cmip6.

Huppmann, D., Rogelj, J., Kriegler, E., Krey, V., & Riahi, K. (2018). A new scenario resource for integrated 1.5 c research. *Nature Climate Change*, *8*(12), 1027–1030. doi: 10.1038/s41558-018-0317-4

Lamboll, R. D. (n.d.). *Modifying emission scenario projections to account for the effects of COVID-19, in prep.*

Lamboll, R. D., Nicholls, Z. R. J., Kikstra, J. S., Meinshausen, M., & Rogelj, J. (2020, May). Silicone v1.0.0: an open-source python package for inferring missing emissions data for climate change research. , 1–23. doi: https://doi.org/10.5194/gmd-2020-138

Pincus, R., Forster, P. M., & Stevens, B. (2016). The Radiative Forcing Model Intercomparison Project (RFMIP): experimental protocol for CMIP6. *Geoscientific Model Development*, *9*(9), 3447–3460. doi: 10.5194/gmd-9-3447-2016

Platnick, S., Hubanks, P., Meyer, K., & King, M. D. (2015). *MODIS Atmosphere L3 Monthly Product (08_L3). NASA MODIS Adaptive Processing System, Goddard Space Flight Center.* doi: http://dx.doi.org/10.5067/MODIS/MOD08_M3.006(Terra),http://dx.doi.org/10.5067/MODIS/MYD08_M3.006(Aqua)

Popp, A., Calvin, K., Fujimori, S., Havlik, P., Humpenöder, F., Stehfest, E., ... Vuuren, D. P. v. (2017). Land-use futures in the shared socio-economic pathways. *Global Environmental Change*, *42*, 331–345. doi: 10.1016/j.gloenvcha.2016.10.002

Ranjan, A. K., Patra, A. K., & Gorai, A. K. (2020). Effect of lockdown due to sars covid-19 on aerosol optical depth (aod) over urban and mining regions in india. *The Science of the total environment*, *745*, 141024–141024. doi: 10.1016/j.scitotenv.2020.141024

Rogelj, J., Shindell, D., Jiang, K., Fifita, S., Forster, P., Ginzburg, V., ... Vilarino, M. V. (2018). Mitigation pathways compatible with 1.5c in the context of sustainable development. In G. Flato, J. Fuglestvedt, R. Mrabet, & R. Schaeffer (Eds.), *Global warming of 1.5 c: an ipcc special report on the impacts of global warming of 1.5 c above pre-industrial levels and related global greenhouse gas emission pathways, in the context of strengthening the global response to the threat of climate change, sustainable development, and efforts to eradicate poverty* (p. 93–174). IPCC/WMO. Retrieved from `http://www.ipcc.ch/report/sr15/`

Smirnov, A., Holben, B. N., Slutsker, I., Giles, D. M., McClain, C. R., Eck, T. F., ... Jourdin, F. (2009). Maritime aerosol network as a component of aerosol robotic network. *Journal of Geophysical Research: Atmospheres*, *114*(D6). doi: 10.1029/2008JD011257

Smith, C. J., Kramer, R. J., Myhre, G., Alterskjær, K., Collins, W., Sima, A., ... Forster, P. M. (2020). Effective radiative forcing and adjustments in cmip6 models. *Atmospheric Chemistry and Physics*, *20*(16), 9591–9618. doi: 10.5194/acp-20-9591-2020

Society, T. R. (2020). *Ammonia: zero-carbon fertiliser, fuel and energy store* (No. 978-1-78252-448–9). Retrieved from `https://royalsociety.org/-/media/policy/projects/green-ammonia/green-ammonia-policy-briefing.pdf`

Stevens, B., Fiedler, S., Kinne, S., Peters, K., Rast, S., Müsse, J., ... Mauritsen, T. (2017). MACv2-SP: a parameterization of anthropogenic aerosol optical properties and an associated Twomey effect for use in CMIP6. *Geosci. Mod. Dev.*, *10*(1), 433–452. doi: 10.5194/gmd-10-433-2017

van Heerwaarden, C. C., Mol, W., Veerman, M., Benedict, I., Heusinkveld, B., Knap, W. H., ... Fiedler, S. (submitted). Covid-19 lockdown contribution to spring surface solar irradiance record in western europe. doi: arXiv:2008.13497

Wyser, K. (2020). *Effective radiative forcing (ERF) experiments with EC-Earth3.* Zenodo. doi: 10.5281/zenodo.4106258

Wyser, K., Kjellström, E., Koenigk, T., Martins, H., & Döscher, R. (2020). Warmer climate projections in EC-Earth3-Veg: the role of changes in the greenhouse gas concentrations from CMIP5 to CMIP6. *Environmental Research Letters*, *15*(5), 054020.

Zuidema, P., Redemann, J., Haywood, J., Wood, R., Piketh, S., Hipondoka, M., & Formenti, P. (2016, 08). Smoke and Clouds above the Southeast Atlantic: Upcoming Field Campaigns Probe Absorbing Aerosol's Impact on Climate. *Bulletin of the American Meteorological Society*, *97*(7), 1131-1135. doi: 10.1175/BAMS-D-15-00082.1